Magnetically Induced Demulsification of Water and Castor Oil Dispersions Stabilized by Fe_3O_4-Coated Cellulose Nanocrystals

Mohammad J. Hasan, Frankie A. Petrie, Ashley E. Johnson, Joshua Peltan, Meredith Gannon, Robert T. Busch, Serhiy O. Leontsev, Erick S. Vasquez, Esteban E. Urena-Benavides*

Authors Information

Mohammad J. Hasan, Esteban E. Urena-Benavides*

Department of Chemical Engineering, University of Mississippi, University, MS, 38677, USA

Department of Biomedical Engineering and Chemical Engineering, The University of Texas at San Antonio, San Antonio, 78249, TX, USA

*Corresponding Author

Email: esteban.urena-benavides@utsa.edu

Mohammad Jahid Hasan ORCID iD: https://orcid.org/0000-0001-5288-650X

Esteban E. Urena-Benavides ORCID iD: https://orcid.org/0000-0002-5525-488X

Frankie A. Petrie, Robert T. Busch, Erick S. Vasquez

Department of Chemical and Materials Engineering, University of Dayton, Dayton, OH, 45469-0256, USA

Erick S. Vasquez ORCID iD: https://orcid.org/0000-0002-4811-6155

Ashley E. Johnson,[a] Joshua Peltan,[a] Meredith Gannon,[a]

Department of Chemical Engineering, University of Mississippi, University, MS, 38677, USA

Serhiy O. Leontsev,
University of Dayton Research Institute, University of Dayton, Dayton, OH, 45469, USA

Abstract Superparamagnetic iron oxide (Fe_3O_4) nanoparticle (NP) coated cellulose nanocrystals (CNCs) were synthesized and used to prepare emulsions with magnetically controlled stability. Magnetite NPs were deposited onto the surface of wood pulp CNCs (WCNCs) and bacterial CNCs (BCNCs) by a one-step coprecipitation method. The effect of the CNC to Fe_3O_4 mass ratio (1:1, 1:2, and 1:4) was varied to optimize the colloidal, magnetic and emulsifying properties of the hybrid NPs. TEM images showed that the 1:4 ratios lead to greater coverage of Fe_3O_4 than lower Fe_3O_4 loadings (1:1, and 1:2). The CNCs and Fe_3O_4 appeared to interact via hydrogen bonding between the hydroxyl groups on the surfaces of both particles. The hybrid NPs had high saturation magnetizations of 56 emu/g for WCNC/Fe_3O_4 (1:4) and 60 emu/g for BCNC/Fe_3O_4 (1:4). In addition, they were efficient stabilizers for castor oil and water emulsions. The magnetite lowered the colloidal stability of the CNCs while providing superparamagnetic properties which allowed stabilization of Pickering emulsions and the subsequent depletion of the Pickering effect by an external magnet. Water-in-oil emulsions, with oil contents of 70% and 90% V/V, were broken by an external magnet, while the CNC/ Fe_3O_4 NPs were recovered and recycled. The 30% and 50% V/V oil emulsions were oil-in-water and could not be broken by the magnet, probably due to higher emulsion stability. The fabricated magnetic CNCs have potential use in magnetically driven separations, drug delivery, and oil recovery.

Keywords *Superparamagnetic cellulose nanocrystals; castor oil; Pickering emulsion; magnetic separation; demulsification*

Introduction

Cellulose nanocrystals (CNCs) are highly crystalline, non-toxic, low-cost, rigid, and green nanomaterials (Roman 2015), which are appealing in a variety of applications like nanocomposites and emulsions. CNCs are generally isolated from various cellulosic sources, including wood (Dong et al. 2016), cotton (Salas et al. 2014) and bacteria (Kalashnikova et al. 2012), by a controlled acid-hydrolysis process. The hydroxyl groups on the surface of CNCs are reactive, which helps chemically modify their surface with organic or inorganic materials (Bendahou et al. 2015). These hydroxyl groups take part of the modification of the CNC surfaces with metal nanoparticles such as platinum (Benaissi et al. 2010), gold (Mahmoud et al. 2013), silver (Kumar et al. 2018) and iron (Dhar et al. 2016) by acting both as nucleating sites and a reductant (Dhar et al. 2015). Recently, studies regarding the deposition of magnetic particles on the CNC surfaces have received substantial attention due to the potential applications in biocatalysis (Cao et al. 2014), magneto-responsive materials (Nypelö et al. 2014b), low-energy separations (Saien et al. 2015), and emulsions (Wang et al. 2013).

There are a few published papers that focused on the synthesis, characterization, and applications of magnetic NP/CNC based composites. Mahmoud et al. (Mahmoud et al. 2013)

synthesized CNC/Fe_3O_4/gold nanocomposite to immobilize papain. Later, Cao et al. (Cao et al. 2014) also synthesized superparamagnetic magnetite (Fe_3O_4) NPs in the presence of non-ionic CNCs and cationic chitosan through the base-catalyzed coprecipitation of iron chlorides to immobilize papain, catalyze the formation of tyrosine and recover the enzyme through a magnetic field. Using cobalt-iron oxide NPs as a metal precursor, Nypelö et al. (Nypelö et al. 2014b) incorporated cobalt-iron oxide particles on the surface of CNCs from the base-catalyzed coprecipitation of $Fe(II)SO_4 \cdot 6H_2O$ and $CoCl_2$, which were used to make self-standing magnetic NP films and polyvinyl alcohol electrospun composites. Olsson et al. (Olsson et al. 2010) synthesized cobalt ferrite, $CoFe_2O_4$, NPs coated bacterial cellulose nanofibrils to prepare magnetic aerogels and nano papers, which were added to magnetically aligned polylactic acid based nanocomposites. Similarly, Garcia et al. (Sanchez-Garcia and Lagaron 2010) prepared cobalt ferrite nanotubes using bacterial cellulose nanofibers, and Tian et al. (Tian et al. 2015) synthesized $Cu_{0.5}Co_{0.5}Fe_2O_4$ coated CNCs via the in-situ hydrothermal reaction for potential biomedical applications

Magnetic cellulose-based materials were used in stabilizing Pickering emulsions (Nypelö et al. 2014b; Low et al. 2017, 2019). Low et al. synthesized Fe_3O_4-cellulose nanocrystals (MCNCs) via ultrasound assisted co-precipitation method to stabilize palm olein-in-water Pickering emulsion (Low et al. 2017). The stability of the emulsions was studied at different pHs. Later, Low et al. reported using Fe_3O_4@cellulose nanocrystals-stabilized Pickering emulsions containing curcumin to magnetically trigger drug release (Low et al. 2019). The hybrid NPs were used to study in-vitro anti-colon cancer. Magnetic CNCs coated by $CoFe_2O_4$ were used in emulsions by Nypelö et al. (Nypelö et al. 2014a) to stabilize hexadecane and toluene emulsions in water and synthesize polystyrene microbeads in situ. The microbeads were used to remove methylene blue from water and were separated by the action of a magnet. Moreover, bare magnetite NPs were also reported to be useful in stabilizing Pickering emulsions (Zhou et al. 2011). Kalashnikova et al. showed that colloidally stable sulfated CNCs failed to stabilize emulsions in water, while CNCs with a low surface charge were effective stabilizers (Kalashnikova et al. 2011, 2012). On the other hand, it was also reported that flocculated sulfated CNCs can stabilize emulsions in ionic strengths higher than 0.6 M (Parajuli et al. 2019, 2020).

In this work, we show that magnetite coated CNCs can provide both, the emulsifying properties from flocculated, anisotropic, and amphiphilic CNCs, as well as the superparamagnetic properties from magnetite NPs. The hybrid NPs have a lower colloidal stability than unmodified CNCs and can be used in stabilizing Pickering emulsions in the absence of salt, and then be separated from the suspension by using an external magnet. Herein, in addition to studying the stabilization of water/castor oil Pickering emulsions by superparamagnetic CNCs, we also study the effectiveness of these NPs to demulsify Pickering emulsions on demand by the action of a permanent magnet.

We synthesized superparamagnetic CNCs by a one-step coprecipitation method using iron salts and CNCs in the presence of NH_4OH. Though hybrid CNC/Fe_3O_4 NPs have been previously synthesized (Cao et al. 2014; Dhar et al. 2016), to the knowledge of the authors, this paper establishes for the first time the use of these particles to stabilize and destabilize Pickering emulsions at will. We derived CNCs from wood pulp (average length 120 ± 70 nm) and bacterial CNCs from nata de coco (average length 505 ± 200 nm) that provided aspect ratios (length/height) of 19.7 ± 15.0 and

66.5 ± 47, respectively. Bare magnetite NPs were incorporated into each type of CNC at different CNC to magnetite ratios (1:1, 1:2 and 1:4). Their physical, chemical and magnetic properties were characterized, as well as their efficacy in stabilizing and demulsifying water/castor oil emulsions. The ability of a magnetic field to stabilize and destabilize Pickering emulsions depended on the magnetite content and the oil to water volume ratio. This paper reports that adequate design of CNC/Fe_3O_4 NPs, and tuning of emulsion conditions, can enable the removal of the superparamagnetic nanoparticles from a liquid/liquid interface via an external magnetic field, thus depleting the Pickering effect and destabilizing emulsions.

Material and Methods

Materials

Southern bleached softwood kraft (SBSK) pulp was kindly provided by Weyerhaeuser pulp mill (Columbus, MS). Nata de coco, as a cellulosic source for bacterial CNCs fabrication, was purchased from Walmart. Sulfuric acid (>96% purity), ammonium hydroxide (28.0 to 30.0 w/w %), Iron (II) chloride tetrahydrate (>96% purity), iron (III) chloride hexahydrate (>97% purity), and amaranth (>85% purity) were all purchased from Thermo Fisher Scientific (Waltham, MA) and were used as received. Castor oil (>99.5% purity) was bought from Sigma Aldrich (St. Louis, MO) and was used as received.

Isolation of wood-pulp CNCs and bacterial CNCs

Southern bleached softwood kraft (SBSK) pulp was used to isolate wood-pulp CNCs (WCNCs), and nata de coco was used as a raw material for bacterial CNCs (BCNCs) isolation. Nata de coco was pretreated to isolate and bleach bacterial cellulose following a procedure by Kalashnikova et al. (Kalashnikova et al. 2012). At first, nata de coco cubes were blended in a Farberware blender (Model: MJ-BL4501AW) at maximum speed. The blended slurry was then added to 0.5 M NaOH in a beaker and stirred for 2 h at 70˚C. The resulting dispersion was centrifuged and washed with deionized (DI) water until pH 7. The obtained solid was bleached twice with an 8.5g/L $NaClO_2$ solution in sodium acetate buffer (pH 4.5) at 70˚C for 2 h. The bleached bacterial cellulose suspension was then centrifuged multiple times until the pH remained stable and then freeze-dried.

Both, SBSK pulp and pretreated bacterial cellulose, were hydrolyzed with 64% sulfuric acid, separately, at 45˚C for 50 min to obtain WCNCs and BCNCs. The isolation process was done as reported in multiple papers (Gray 2008; Ureña-Benavides et al. 2010, 2011). In short, the hydrolysis reactions were quenched with cold DI water. The suspensions were allowed to precipitate, and the supernatants were poured out. Then the excess acid from both CNC suspensions

was removed by centrifugation and the particles washed using DI water. The centrifuged suspensions were then dialyzed using a RC dialysis membrane (3.5 kDa MWCO) against DI water for several days until constant pH to remove remaining excess acid. Both CNC suspensions were then sonicated by an ultrasonic horn (QSonica; Q700) to redisperse CNCs and were then stored in a refrigerator for later use.

Size Measurement of WCNCs and BCNCs

The morphology of the neat WCNCs and neat BCNCs was observed by a MultiMode 8 atomic force microscope AFM from Bruker Nano, Inc. (Billerica, MA) in tapping mode with probes obtained from Ted Pella, Inc. (Tap300-G silicon probe, <10 nm tip radius, 300 kHz resonance frequency, and 40 N/m spring constant). One drop of suspensions (0.0001%) was placed onto a freshly cleaved mica surface obtained from Ted Pella Inc. (V1 AFM Mica Discs, 10 mm diameter) and dried in a desiccator overnight. The dimensions of the nanoparticles were determined by AFM imaging using the software Gwyddion (version 2.55) (Parajuli et al. 2019).

Sulfur Content Measurement of CNCs

The sulfur content ($-SO_3H$) in both CNC surfaces was measured by conductometric titration (Abitbol et al. 2013) of their aqueous suspensions. A 0.05 wt% CNC aqueous suspension (120 ml) was dispersed by probe sonication for 3 minutes (Amplitude: 30; 1 min on and 1 min off) in an ice bath. Then the CNCs were titrated with a 1.25 mM NaOH solution. The pH and conductivity of the suspension were monitored by a benchtop Orion Star A215 multiparameter meter (Thermo Scientific, Waltham, MA). The sulfur content on the surface of CNCs was determined by using the following equation (Dong et al. 1998; Abitbol et al. 2013):

$$\%S = \frac{V_{NaOH} * C_{NaOH} * M_w(S)}{m_{susp} * C_{susp}} \times 100\% \quad (1)$$

Synthesis of Magnetite coated Cellulose Nanocrystals (CNC/Fe_3O_4)

Magnetite NPs were coated onto CNCs by coprecipitation of iron chloride salts with a weak base (NH_4OH). Existing methods for the fabrication of Fe_3O_4 were modified to prepare the hybrid nanoparticles (Xue et al. 2014; Ureña-Benavides et al. 2016; Dhar et al. 2016). The reactions were done with theoretical mass compositions of CNC/Fe_3O_4 of 1:1, 1:2, and 1:4, to determine which provides the best colloidal and magnetic properties, in addition to adequate emulsification capacity.

To prepare WCNC/Fe_3O_4 at 1:4 ratio, 1.875 g WCNCs were dispersed into 400 ml DI water of pH 10, followed by probe sonication for 5 minutes (Amplitude: 30; 1 min on and 1 min off). Then

6.4 g iron (II) chloride tetrahydrate and 15.78 g iron (III) chloride hexahydrate were dissolved in 100 ml DI water. Both of the above solutions were degassed by sparging with N_2. The iron chloride salts solution was added dropwise to the WCNC suspension under a N_2 atmosphere, in an RB flask at 90 ˚C, while stirring with an overhead stirrer (Fisherbrand, Fisher Scientific) at 1000 rpm and maintained at that temperature for 2 h with continuous N_2 purging. After 2h, 75 ml NH_4OH was added dropwise to the mixture; the dispersion turned black immediately. The reaction was run for another 2 h with the same operating conditions. Upon completion, the reaction mixture was allowed to cool down, the NPs were separated by a 2"×2"×1" Neodymium permanent magnet (Applied Magnets, Grade N52, 14800 Gauss) and washed three times with DI water to remove the impurities. Similarly, for preparing WCNC/Fe_3O_4 of 1:1 and 1:2, 7.5 g and 3.75 g WCNCs were used, respectively, in the coprecipitation reaction. The rest of the procedures remained the same. BCNC/Fe_3O_4 of 1:1, 1:2, and 1:4 were synthesized using the same procedure.

Synthesis of Bare Magnetite Nanoparticles

Bare magnetite NPs were synthesized by coprecipitation of iron chloride salts with NH_4OH, modifying the method described by Xue et al. (Xue et al. 2014). Citrate was not used to coat the magnetite NPs to make a direct comparison of the properties with hybrid magnetic CNCs. A detailed procedure of bare magnetite NPs preparation is provided in the supporting information.

Characterization of MagCNC NPs and bare magnetite NPs

Transmission Electron Microscopy (TEM) images were acquired using a Hitachi H-7600 TEM operated at 100 kV. A diluted suspension of the respective MagCNCs was used to prepare the samples. A microdroplet (~ 5 microliter) of the suspension was deposited onto a copper carbon mesh grid (CF300-Cu grids, Electron Microscopy Science) and allowed to dry inside a ventilated hood for at least 24 h prior image collection.

The thermal decomposition of the WCNCs, BCNCs, Fe_3O_4 NPs and CNC/Fe_3O_4 was determined by a thermogravimetric analyzer (Q500, TA Instruments, New Castle, DA). Freeze-dried samples (5 to 10 mg) were heated on a TGA pan from room temperature up to 600°C under nitrogen with a heating rate of 10°C/min (Kumar et al. 2018). These measurements were used to calculate the amount of Fe_3O_4 present in the modified CNCs from the difference in residual weight (RW) of WCNCs, BCNCs, Fe_3O_4 NPs, and the hybrid CNC/Fe_3O_4 at 600˚C by using equation 2.

$$Magnetite\ Content\ (\%) = \frac{RW_{\mathrm{CNC}/Fe_3O_4} - RW_{CNC}}{RW_{Fe_3O_4} - RW_{CNC}} \times 100\ \% \quad (2)$$

Here the subscript represents the type of nanoparticle being considered. A detailed calculation is provided in the supporting information document.

Magnetization data of WCNC/magnetite (1:4) and BCNC/magnetite (1:4) were acquired using a vibrating sample magnetometer (VSM) at room temperature and applied magnetic field up

to 3T (Quantum Design Versalab). For bare magnetite NPs, WCNC/magnetite (1:1), and WCNC/magnetite (1:2) samples, a Lakeshore VSM with 2T max field was utilized. Weighted amounts of each samples were used, and the normalized moment (emu/g) is reported for each sample as a function of magnetic field.

Fourier Transform Infrared (FTIR) spectra of the freeze-dried WCNCs, BCNCs, MagCNCs, and bare magnetite NPs were obtained with a spectrometer (Cary 630 FTIR spectrometer, Agilent Technologies) using an attenuated total reflectance (ATR) sampling mode with a single-bounce diamond crystal. The spectrum range was 4000- 600 cm^{-1} with a resolution of 4 cm^{-1}.

Raman spectra of the samples were acquired with a solid-state Horiba Labram HR Evolution Raman (Horiba Instruments Inc, TX) using 532 nm laser excitation and 600 grooves/mm grating.

The zeta potential and Z-average hydrodynamic diameter of the neat CNCs, bare magnetite NPs, and MagCNCs were measured with a Malvern Zetasizer Nano ZS (Malvern Instruments, UK). A low concentration (0.1 wt%) of each sample was prepared and the measurements were done at pH 7.

The colloidal stability of neat CNCs and MagCNCs in water was investigated using a UV-Visible spectrophotometer (Genesys 150, Thermo Scientific). Aqueous suspensions (10 ml) of CNCs and MagCNCs at various concentrations (0.001 wt% to 0.1 wt%) and pH 7 were prepared from their mother suspensions and kept in vials. The photographs of the vials were taken at 0, 1, and 7 days and the stability of the dispersions was visually inspected. The stability of the dispersions was also analyzed by the UV-Visible spectrophotometer within the wavelengths of 200 nm to 800 nm during the same timeframe monitoring the change in absorbance.

Preparation of castor-oil/ water Pickering emulsions

Pickering emulsion of castor oil and water, stabilized by the hybrid CNC/Fe_3O_4 NPs, were prepared by mixing the castor oil with the aqueous suspension. At first, 100 ml 1 wt% aqueous suspension was prepared. Then the required amounts of suspension and castor oil were added to vials so that the total volume of each emulsion was 10 ml. The samples were mixed thoroughly with a high shear mixer (IKA Ultra-Turrax T-25 Basic, Atkinson, NH) at 9000-10000 rpm for 2 minutes. Once emulsions were prepared, pictures of the vials were taken at 0 h and 24 h with a digital camera to monitor emulsion creaming. Microscopic pictures of the emulsions were also taken using an optical microscope (AmScope 500MD), and droplet size distributions were determined by measuring at least 100 droplets with Image J. Both WCNC/Fe_3O_4 and BCNC/Fe_3O_4 at a 1:4 ratio, were used separately to prepare emulsions. Castor oil to water volume ratios (v/v) of 30/70, 50/50, 70/30 and 90/10 were investigated.

Demulsification of Castor-oil/ Water Pickering emulsions

Demulsification of the Pickering emulsions made with castor oil, water, and MagCNC NPs was investigated under the presence of an external magnetic field. Briefly, the vials of the emulsions were put on a neodymium N52 grade magnet (Applied Magnets, AOM05648221) that has a high residual magnetic flux density (14800 gauss). The effect of the magnetic field on demulsifying the emulsions was tested by taking photographs of the vials using a digital camera at 0 h and 24 h. Microscopic images of the emulsion droplets were simultaneously taken using an optical microscope (AmScope 500MD), and droplet size distributions were calculated by scaling at least 100 droplets with ImageJ software.

Results and discussion

Morphological, thermal and chemical characterization of magnetite coated CNCs (CNC/Fe_3O_4)

Magnetite NPs were incorporated onto the surface of WCNC aggregates with theoretical mass ratios (WCNC/Fe_3O_4) of 1:1, 1:2, and 1:4 by a one-step coprecipitation reaction. The original individual WCNCs had average lengths of 120 ± 70 nm, and heights (width) of 6.1 ± 3 nm, as indicated in supporting information Figure S1, and a sulfur content of 0.41 ± 0.05% (g-sulphur/100 g-cellulose) as indicated in supporting information Figure S2. The bare magnetite NPs had average diameters of 19.81 ± 3.4 nm (Fig. S3). Magnetite NPs are generally coated with organic materials to control their growth and stability (Cîrcu et al. 2016). In this work, the magnetite NPs were stabilized by CNCs, although aggregation of magnetite was evident. Figure 1 shows the successful deposition of magnetite NP clusters (dark spheres) onto the lighter, elongated, CNC aggregates. Free magnetite NPs could not be found in the images; in all cases, the Fe_3O_4 NP clusters appeared to be connected to CNCs. Although the 1:1 WCNC/Fe_3O_4 NPs showed large proportions of uncovered CNC surface (Fig. 1a). As the magnetite to cellulose ratio increases, the coverage appears to increase (Fig. 1b and 1c), decreasing the amount of exposed CNC surface. BCNC aggregates were also coated with Fe_3O_4 NP clusters with a theoretical composition of 1:1, 1:2, and 1:4. In this case, the original individual BCNCs were 505 ± 200 nm long by 7.6 ± 4.5 nm wide and had sulfur contents of 0.24 ± 0.04% in BCNCs (Fig. S1 and S2). TEM images of 1:1 BCNC/Fe_3O_4 and 1:2 BCNC/Fe_3O_4 are shown supporting information Figure S3, while Figure 1d shows the 1:4 BCNC/Fe_3O_4 NPs. BCNC coverage by Fe_3O_4 also increased as the theoretical ratio increased. TEM images of the hybrid NPs appear to indicate BCNCs had better magnetite coverage, which may be a consequence of the lower area to mass ratio compared to WCNCs. The aggregation of CNCs is driven by the presence of iron salts during the synthesis of Fe_3O_4 NPs, while magnetite aggregates given that the only stabilizing

agent are the CNCs themselves. Even though aggregation of both nanomaterials is evident, this state is particularly helpful in applications like emulsion stabilization and magnetically-induced separations (Midmore 1998; AlYousef et al. 2018; Parajuli et al. 2019).

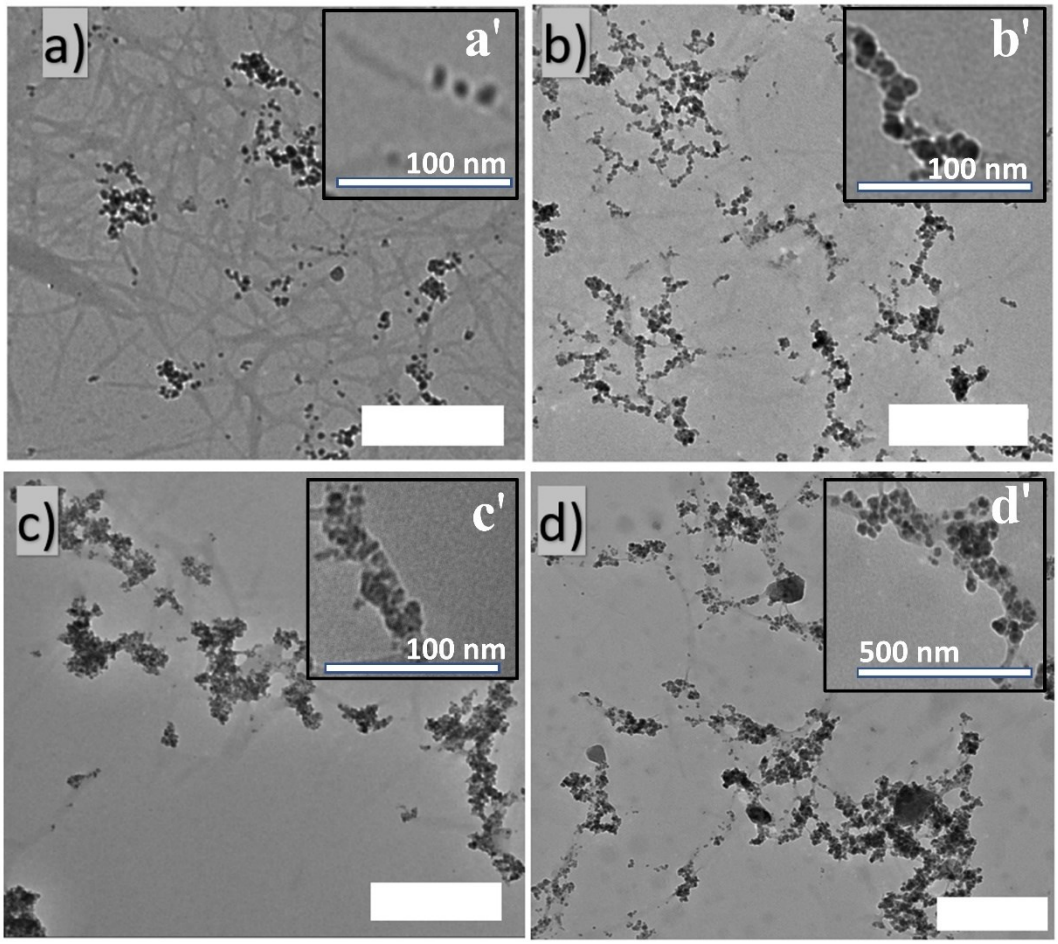

Fig. 1 Transmission electron micrograph of **a** WCNC/Fe_3O_4 of 1:1; **b** WCNC/Fe_3O_4 of 1:2; **c** WCNC/Fe_3O_4 of 1:4, **d** BCNC/Fe_3O_4 of 1:4; Thick scale bars on a, b, c, and d represent 500 nm; Insets a′, b′, c′, and d′ shows higher magnified images.

Magnetite content of all hybrid NPs was determined by TGA. Figure 2 shows TGA traces of bare magnetite nanoparticles, bare CNCs, and the different magnetite coated CNCs. In samples containing CNCs, the particles initially lost weight between 100˚C and 200˚C due to the removal of moisture and sulfate groups present on the surface, the remaining degradation occurred between 200˚C and 600˚C, and is due to the decomposition of the cellulose chains. In the case of bare Fe_3O_4 NPs, a negligible amount of weight loss (~ 3 %) was observed within the temperature range studied. Increasing the magnetite concentration in the modified WCNCs and modified BCNCs, increased their thermal stability compared to the bare WCNCs and bare BCNCs, respectively. The actual amount of CNCs and Fe_3O_4 present in the modified CNCs was calculated from the difference in weight loss of bare WCNCs, bare BCNCs, and the modified CNCs at 680˚C and is presented in Table 1. A detail procedure of the magnetite content calculations from the TGA graph is given in supporting information (page 6). It was found that WCNC/Fe_3O_4 at 1:1, 1:2, and 1:4 ratios, and BCNC/Fe_3O_4 at 1:4 had magnetite contents of 53.3 ± 5.1%, 66.0 ± 6.9%, 73.0 ± 6.0% and 66.84 ±

5.1% respectively. These values were close to the theoretical contents of 50%, 66.7%, 80%, and 80%, based on the amounts added to the reaction mixture, indicating a minimal loss of CNCs during the purification steps, as well as good attachment of magnetite NPs. Notably, the lowest CNC:magnetite ratios (1:4) gave lower magnetite contents than expected. This result could be due to smaller Fe_3O_4 NPs not attaching onto the CNCs. All reaction mixtures had the same magnetite concentration, while the different ratios were obtained by lowering CNC content. The 1:4 reactions had the lowest CNC amounts; it is possible those CNCs were saturated with magnetite preventing additional adsorption. It is also possible that small NPs of less than 20 nm may show strong Brownian motions that prevent their adsorption onto CNCs. It is expected that some of those Fe_3O_4 NPs could remained in suspension and lost during purification due to being less strongly attracted to the external magnet (Berg 2010).

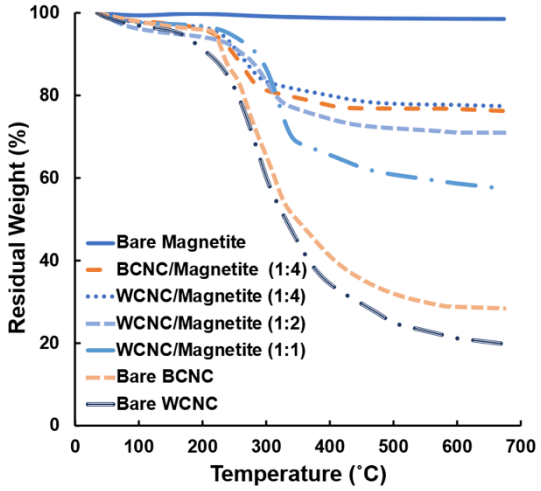

Fig. 2 Thermogravimetric Analysis (TGA) of representative traces of bare Fe_3O_4, BCNC/Fe_3O_4 (1:4), WCNC/Fe_3O_4 (1:4), WCNC/Fe_3O_4 (1:2), WCNC/ Fe_3O_4(1:1), bare BCNCs, and bare WCNCs

Table 1 Experimental percentage of CNCs and Fe_3O_4 in the prepared magnetic CNCs

Experimental (%)	WCNC/Fe_3O_4 (1:1)	WCNC/Fe_3O_4 (1:2)	WCNC/Fe_3O_4 (1:4)	BCNC/Fe_3O_4 (1:4)
% of CNC	46.7 ± 10.2	34.0 ± 6.9	26.9 ± 6.1	33.1 ± 5.1
% of Fe_3O_4	53.3 ± 10.2	66.0 ± 6.9	74.1 ± 6.1	66.9 ± 5.1

The chemical composition of modified CNCs was further studied by FTIR spectroscopy and was compared with neat CNCs and Fe_3O_4 (Fig. 3 and Fig. S3). Both neat WCNCs and neat BCNCs showed characteristic typical cellulose absorption peaks at ~3333, 2896, 1654, 1428, 1315, 1163, 1050, 898 cm^{-1} corresponding to -OH stretching bonds, symmetric C-H stretching vibration, -OH bending, asymmetric angular deformation of C-H, -CH_2 wagging, asymmetrical C-O-C glycoside bonds, and C-OH stretching in plane at C6, and the -C-O-C asymmetric bending, consistent with existing literature (Dhar et al. 2016; Wardhono et al. 2018). The peak at 3333 cm^{-1} is overlapped with a weak vibration at 3450 cm^{-1} corresponding to free -OH groups on the surface of the CNCs. Magnetite coated CNCs also showed all characteristics peaks of CNCs, although with

lower relative intensities, due to the lower concentration of CNCs in the hybrid NPs. In the modified CNCs, the -OH stretching peak at 3333 cm^{-1} was found to be broader, and of lower intensity compared to the original CNCs. These characteristics suggest increased hydrogen bonding of the hydroxyl groups, which appears to drive the interaction between magnetite and CNCs.

The presence of magnetite on the CNC surface was further confirmed by Raman spectroscopy (Fig. S5). Hybrid WCNC/Magnetite (1:4) NPs had the characteristics peak at 690 cm^{-1} which confirmed the presence of magnetite NPs in the hybrid NPs (Shebanova and Lazor 2003) . The peaks at 585 cm^{-1} and 381cm^{-1} indicate the formation of maghemite via oxidation of magnetite by the laser during the Raman measurements (Shebanova and Lazor 2003). Raman spectroscopy of magnetite is challenging and must be done at very low laser power to reduce oxidation to maghemite, as a consequence, the vibration bands of CNCs are almost absent in the hybrid nanoparticles.

It is uncertain if the growth of the Fe_3O_4 NPs occurs directly from the surface of the CNCs, or if they are first formed in the liquid phase and then adsorb onto the cellulosic hydroxyl groups. Before the coprecipitation reaction, negatively charged sulfate groups of CNCs are expected to interact electrostatically with the positively charged iron salts (Fe^{2+} and Fe^{3+}). However, iron salts also have a high binding constant with hydroxyl groups (Dhar et al. 2015). So, the addition of ammonium hydroxide to the reaction mixture may lead to growth of Fe_3O_4 NPs directly from the hydroxyl and possibly the sulfate groups on the CNC surface. However, the shift in the -OH peak position is more prominent for the 1:4 sample in Figure 3 compared to 1:1 CNC/Fe_3O_4. It is thus possible that a second mechanism occurs where free iron salts in solution react to form magnetite. These are known to partially hydrate to yield -OH groups on the NP surface. Those hydroxyl group would also have tendency to hydrogen bond with the CNC surface. Additional experimentation would be needed to study the different potential pathways for the coating of CNCs with Fe_3O_4 NPs.

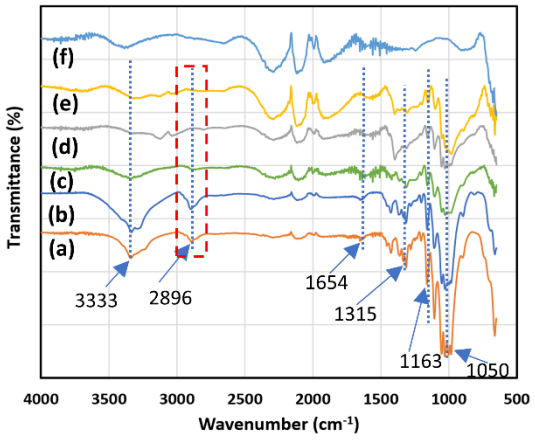

Fig. 3 Fourier transform infrared (FTIR) spectra of **(a)** WCNCs; **(b)** BCNCs; **(c)** WCNC/Magnetite (1:1); **(d)** WCNC/Magnetite (1:4); **(e)** BCNC/Magnetite (1:4); and **(f)** Bare Magnetite NPs.

Colloidal stability of superparamagnetic CNC nanoparticles

The colloidal stability of the CNC/Fe_3O_4 hybrids was investigated in DI water at pH 7 by visual inspection and UV-vis spectroscopy (Fig. 4). Zeta potential and Z-average hydrodynamic diameters of the NPs were also measured to assess colloidal stability (Table 2). UV-vis was used as an indication of the amount of CNCs dispersed in water before precipitation, which indirectly correlates to a lack of colloidal stability. Generally, WCNCs were very stable in water due to the negatively charged sulfate groups on their surface, that provided a highly negative zeta potential (-52.1±14.2 mV). There was no precipitation of WCNCs after 1 week, indicating a very stable aqueous suspension of WCNCs. This was evident by visual inspection and by the absence of significant changes in the absorbance of the WCNCs from 200 to 800 nm within the timeframe studied (Fig. 4a). Bacterial CNCs had a less negative average zeta potential (-42.4 mV± 6.6) than WCNCs (Table 2), but the difference was within the experimental error and both were found to long term colloidal stability. On the contrary, the bare Fe_3O_4 nanoparticles precipitated after 24 h, leading to a substantial drop in absorbance to near zero for the entire wavelength range studied (Fig. 4b). The zeta potential of the bare Fe_3O_4 NPs was measured to be -21.3±3.7 mV which is not negative enough to maintain long term colloidal stability. The data was consistent to the published paper by Soares et al. (Soares et al. 2019).

The hybrid CNC/Fe_3O_4 NPs had more negative zeta potential than bare magnetite NPs and showed better dispersibility. At 0.005 wt%, WCNC/Fe_3O_4 (1:2, and 1:4 ratios) and BCNC/Fe_3O_4 (1:4 ratio) remained stable for 24 hours but precipitated over a week (Figs. 4d, e, f). In all those cases, the absorbance decreased significantly, but it was more significant for BCNC/Fe_3O_4 (1:4), dropping to zero. It was found that WCNC/Fe_3O_4 with a 1:1 ratio was stable for an entire week at a concentration of 0.005 wt% (Fig. 4c). BCNC/Fe_3O_4 of of 1:1, and 1:2 also found to be colloidally stable for over a week (Fig. S6). Increasing the magnetite content of the hybrid NPs resulted in the zeta potential becoming less negative, for WCNC/Fe_3O_4 (1:4), and BCNC/Fe_3O_4 (1:4) they were found to be -32.6 ± 4.8, and -31.6 ± 3.7 mV, respectively (Table 2). Since the CNC/Fe_3O_4 NPs prepared with a 1:4 ratio show good stability for 24 hours and flocculated, these can be useful to prepare Pickering emulsions, where only short term colloidal stability is desired (Midmore 1998; AlYousef et al. 2018; Parajuli et al. 2019).

Colloidal stability of the nanoparticles was also studied by analyzing the hydrodynamic diameter of the NPs in aqueous suspensions at pH 7 by dynamic light scattering (DLS) (Table 2). Though DLS measurements are most useful in analyzing spherical nanoparticles and not very accurate for rod-like particles, it provides a good qualitative assessment of the particles size changes over time. Bare magnetite NPs were found to be aggregated so quickly and the size increased from 32.4 ± 6.5 nm to 1736 ± 199 nm in 2 h. Both WCNCs and BCNCs, on the other hand, were stable for 2 h showing negligible changes in particle size. Hybrid CNCs of 1:1, 1:2, and 1:4 ratios, had an intermediate increase in particle size after 2h, as indicated in Table 2, which demonstrated better colloidal stability than bare magnetite, but lower than WCNCs and BCNCs. Moreover, it was observed the hydrodynamic diameters, immediately after dispersion, clearly increase as the Fe_3O_4 content was raised indicating that higher loads of magnetite lead to more aggregated samples immediately after preparation. In addition, the size distributions of the hybrid CNC/Fe_3O_4 NPs

showed only one population which indicated there was no, or an undetectable, amount of free magnetite in the dispersions (Fig. S7).

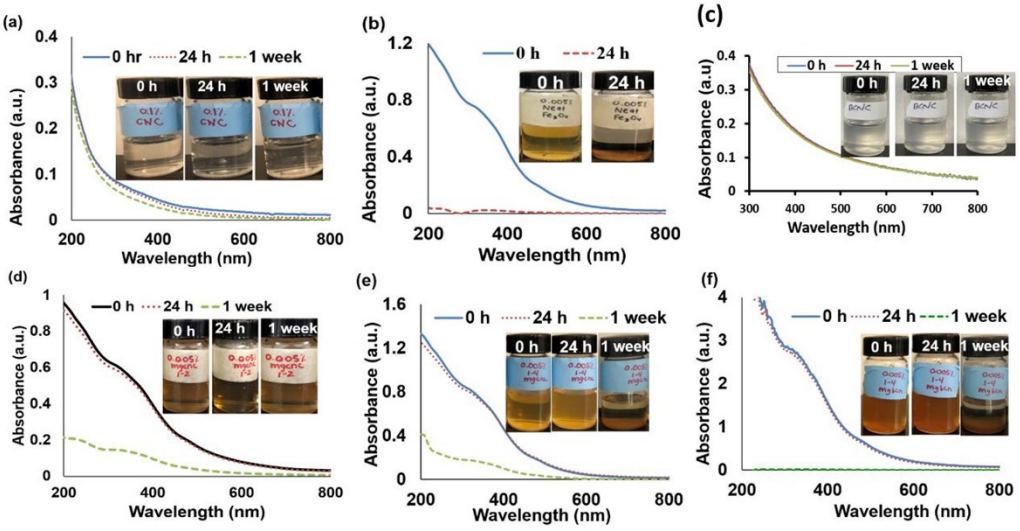

Fig. 4 Colloidal stability of the nanoparticles in DI water at pH 7. **a** neat WCNCs; **b** bare magnetite nanoparticles; **c** neat BCNCs; **d** WCNC/Magnetite (1:2); **e** WCNC/Magnetite (1:4); **f** BCNC/ Fe_3O_4 (1:4). Colloidal stability of the particles was inspected by the visual inspection of the vials and by the UV-vis spectroscopy at 0 h, 24 h, and 1 week.

Table 2 Zeta potential and Z-average hydrodynamic diameter of bare CNCs and magnetic CNCs

Sample names	Zeta Potential (mV)	Z-average hydrodynamic diameter (nm)	
		At time 0 h	After 2 h
Bare WCNC	-52.1 ± 14.2	97.4 ± 0.6	99.7 ± 0.9
Bare BCNC	-42.4 ± 6.6	111.3 ± 1.0	112.7 ± 1.2
Bare Fe_3O_4	-21.3 ± 3.7	32.4 ± 6.5	1736 ± 199
WCNC/ Fe_3O_4 (1:1)	-39.4 ± 3.5	150.2 ± 1.8	243.1 ± 3.2
WCNC/ Fe_3O_4 (1:2)	-37.0 ± 3.9	158.5 ± 0.5	165.7 ± 1.7
WCNC/ Fe_3O_4 (1:4)	-32.6 ± 4.8	227.7 ± 5.3	307.6 ± 6.8
BCNC/ Fe_3O_4 (1:1)	-33.0 ± 6.2	139.3 ± 0.5	145.8 ± 2.1
BCNC/ Fe_3O_4 (1:2)	-32.4 ± 4.6	158.5 ± 0.6	173.8 ± 3.8
BCNC/ Fe_3O_4 (1:4)	-31.6 ± 3.7	367 ± 24	406 ± 13

Castor oil/Water Pickering emulsion

Castor oil contains triglyceride of various fatty acids which consist of approximately 80-90% ricinoleic acid (Keera et al. 2018). However, free fatty acids (FA), monoglycerides (MG) and diglycerides (DG) in castor oil are surfactants and can stabilize emulsions as indicated in Figure 5a. It was found that high shear mixing of castor oil and water formed water in oil (w/o) type emulsion (Fig. 5b and Fig. S8) at various oil to water volume ratios. The emulsion types were determined by using the dye amaranth (Fig. S9). The MG and DG have long hydrophobic tails and small

hydrophilic headgroups, which is likely the reason why the emulsions without NPs are all W/O. These emulsions had significant creaming over 24 h, especially with low oil contents of 30% and 50%. In the presence of neat WCNCs the stability of the water-in-castor oil emulsions was even lower than without nanoparticles. Only at 70% and 90% oil, could an emulsion be formed in the presence of neat WCNCs; these were found to be W/O and remained stable for 24 hours (Fig. 5c and Fig. S10). At 30% and 50% oil, a small, emulsified interface formed which mostly separated within 24 h. However, the oil-rich phase at the top contains some water droplets after 24 hours (Fig. S10). CNCs, generally, adsorb onto the oil water interface to stabilize O/W emulsion as shown in Figure 5a (Parajuli et al. 2019). However, in this case, since castor oil has free fatty acids, and the aqueous phase is salt free, it became harder to emulsify the two phases by the CNCs, especially at lower oil contents. At high oil content, it was easier to emulsify only W/O because there were more fatty acids available as surfactants and also because there was less water to disperse. However, the hybrid CNC/Fe_3O_4, that have been synthesized in this work, do stabilize O/W emulsion. It is believed the magnetite helps adsorb the hybrid NPs onto the oil/water interface. A detail study of the castor oil and water Pickering emulsions stabilization and demulsification are given in the following sections.

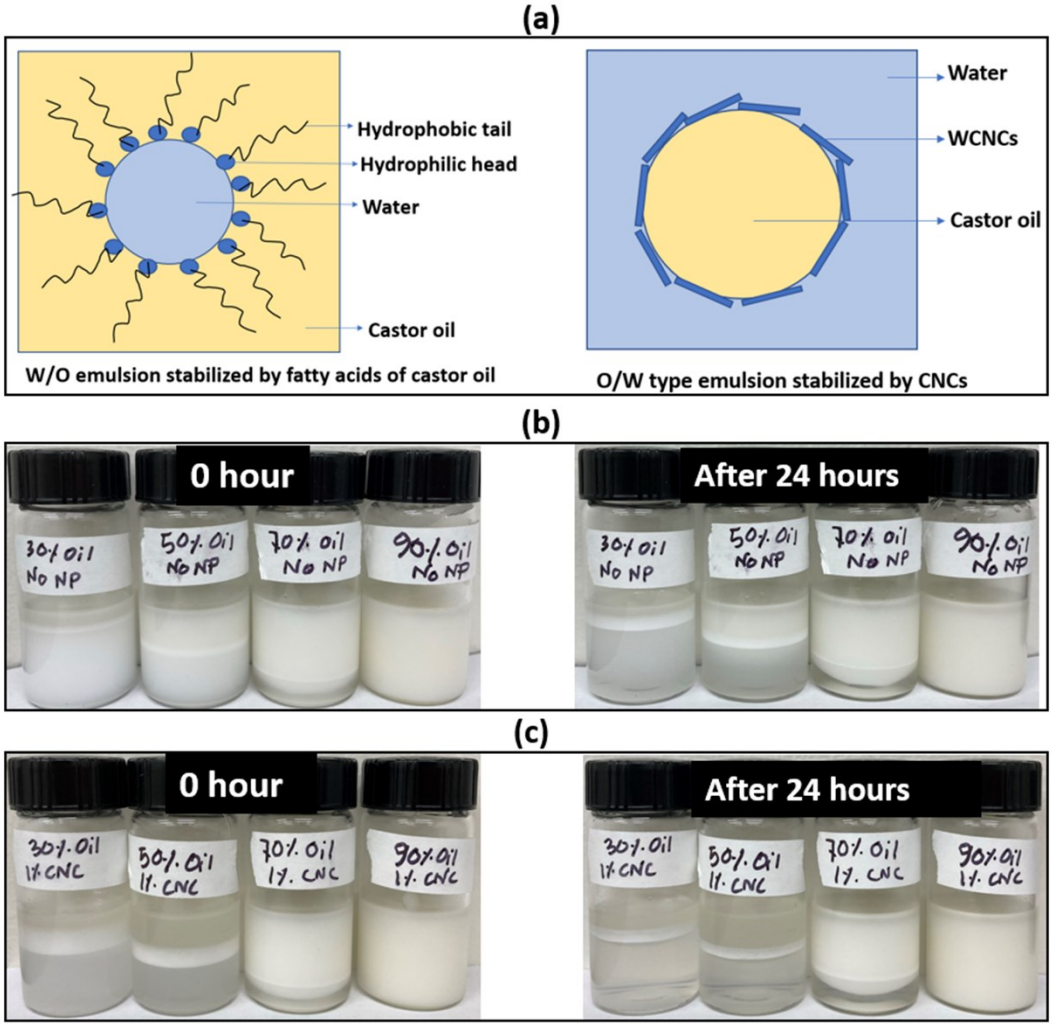

Fig. 5 a Schematic representation of W/O (left) and O/W (right) emulsions stabilized by monoglycerides and diglycerides (W/O), or WCNCs (O/W); **b** picture of the emulsions when

"NO" nanoparticles were used at various oil concentration at time 0 h (left) and after 24 h (right); **c** WCNC stabilized castor oil water Pickering emulsions

Magnetic properties of the CNC/Fe_3O_4 NPs and Pickering emulsion stability

The magnetic properties of the synthesized magnetite coated CNCs were determined using a vibrating sample magnetometer (VSM) and compared with bare Fe_3O_4 nanoparticles. The magnetization curves (Fig. 6a) showed that the saturation magnetization (M_s) of the hybrid MagCNC NPs was lower than the bare Fe_3O_4 nanoparticles (77 emu/g). Among the modified CNCs, BCNC/Fe_3O_4 of 1:4 had the highest M_s (60 emu/g) followed by the WCNC/ Fe_3O_4 with ratios of 1:4 (56 emu/g), 1:2 (43 emu/g), and WCNC/Fe_3O_4 1:1 (31 emu/g). Increasing the magnetite concentration increased the saturation magnetization (Fig. 6b) of the wood pulp based CNCs, indicating successful immobilization of Fe_3O_4 nanoparticles on the surface of CNCs. The linear relationship between M_s and magnetite content indicates the properties of the Fe_3O_4 NPs were not negatively affected by the deposition onto the CNCs. The hybrid MagCNC NPs showed superparamagnetic behavior similar to bare magnetite, analogous to similar particles reported in literature (Lopez et al. 2010; Chen et al. 2014). The magnetization curves had near-zero remanence and coercivity, thus avoiding any hysteresis loop. The longer BCNC/Fe_3O_4 1:4 appeared to have a higher M_s compared to the wood-based CNCs at a similar same magnetite load, which suggests the elongated shape have a tendency to increase the magnetization. However further experimentation would be needed to study the effect of aspect ratio in depth.

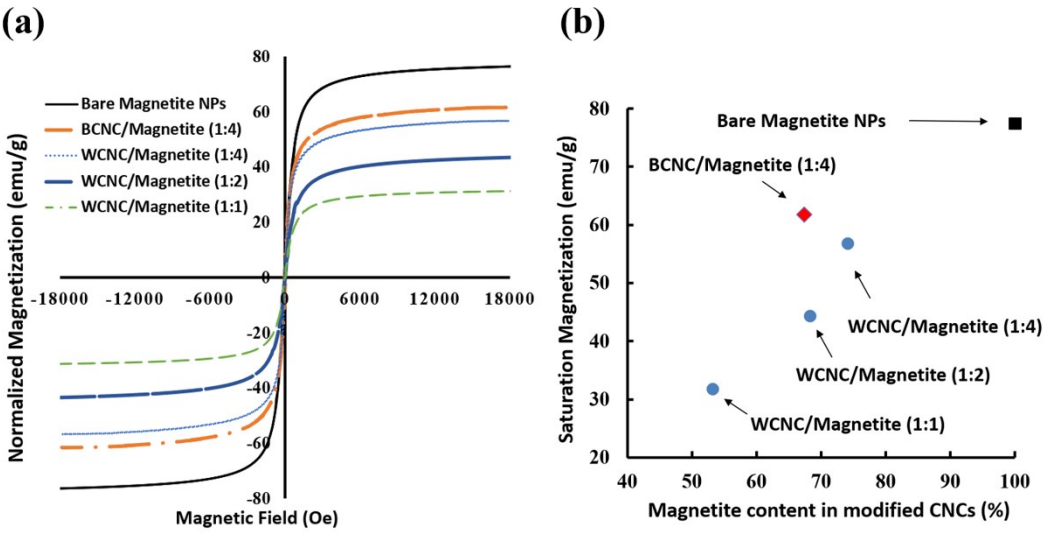

Fig. 6 a VSM magnetization curves of bare magnetite NPs and magnetic CNCs; **b** graph of saturation magnetization (from VSM) vs. magnetite content of modified CNCs (from TGA).

The Fe_3O_4-coated CNCs were used to stabilize castor oil and water Pickering emulsions. Since the modified CNCs of 1:4 had the highest magnetic susceptibility along with moderate

colloidal stability, only WCNC/Fe_3O_4 (1:4) and BCNC/Fe_3O_4 (1:4) were used. Figures 7a and 7b show the pictures of castor oil and water emulsions immediately after preparation (time 0 h) and after 24 h, while the corresponding microscopy images are presented in Figures 7c and 7d. In both cases, all the emulsions remained stable for 24 h, and droplet sizes were almost unchanged (Fig. S11), with the exception of the 50/50 volume ratio where droplet coalescence was detected. It was observed that for castor-oil and water volume ratios of 30/70 and 50/50, the emulsions were oil-in-water (o/w), while for volume ratios of 70/30 and 90/10, the emulsions were water-in-oil (w/o). The emulsion types were determined by dissolving the water-soluble dye amaranth in the aqueous component (Fig. S12).

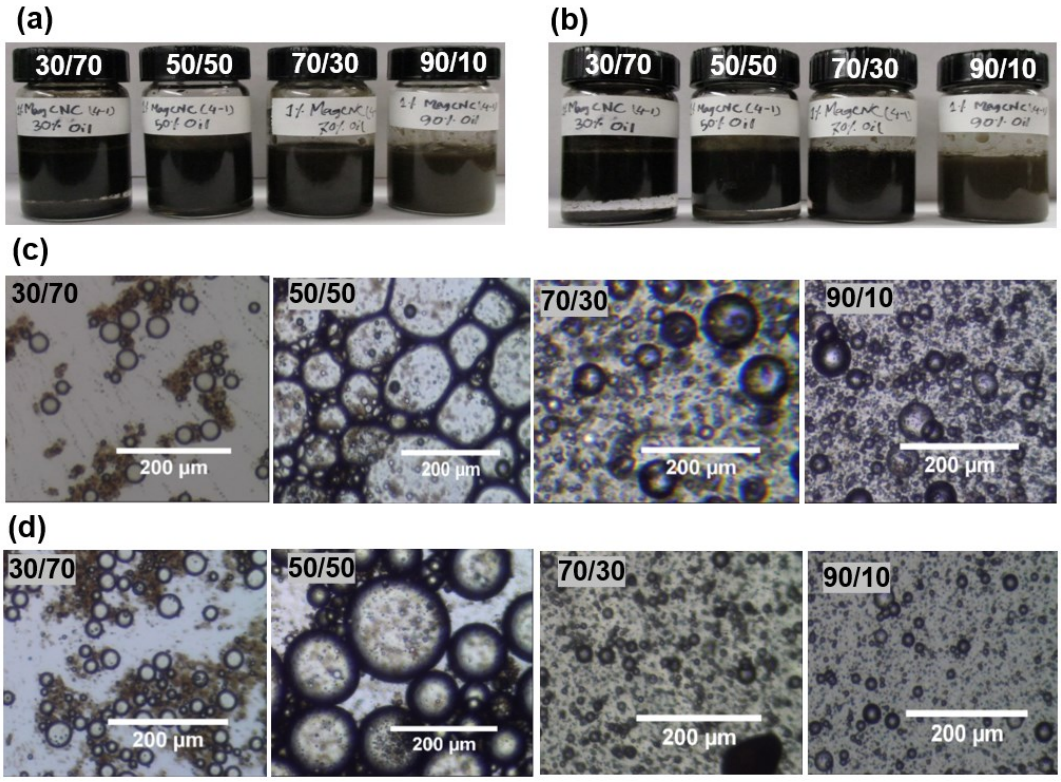

Fig. 7 Pickering emulsions of castor oil and water using WCNC/Fe_3O_4 of 1:4 (1 wt% of aq. phase) and castor oil and water volume ratio (v/v) of 30/70, 50/50, 70/30 and 90/10 (left to right). **a** Picture taken at time 0 h; **b** picture taken after 24 h; **c** corresponding microscopic pictures of the emulsions at time 0 h; **d** microscopic pictures taken after 24 h; Scale bars represent 200 µm.

Similar results were seen with castor oil and water Pickering emulsions stabilized with BCNC/Fe_3O_4 of 1:4 (Fig. 8). The emulsion conditions were maintained the same; it was observed that these emulsions were stable for over 24 hours. BCNC/Fe_3O_4 stabilized emulsions experienced less creaming after 24 h (Fig. 8b) than WCNC/Fe_3O_4 stabilized emulsions (Fig. 7b), suggesting the formation of more stable emulsions with BCNC/Fe_3O_4 NPs. The corresponding microscopic pictures of these emulsions are shown in Figure 8c-d. It should be noted that the aqueous phase that settles at the bottom of the WCNC/Fe_3O_4 stabilized emulsions (Fig. 7b) is transparent, indicating that most of the NPs remained at the interphase in the emulsion phase. In Pickering emulsions, the particles

form a rigid structure around the droplets preventing droplet coalescence and stabilizing the emulsions for extended periods time (Eskandar et al. 2007; Barnes and Gentle 2011).

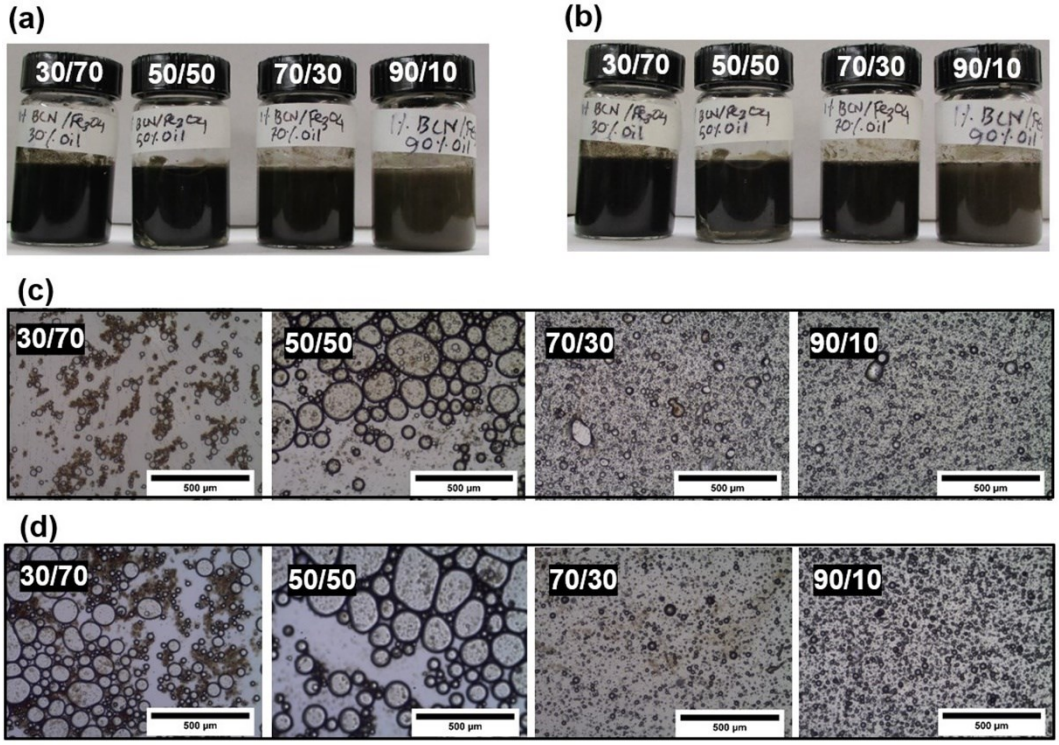

Fig. 8 Pickering emulsions of castor oil and water using BCNC/Fe_3O_4 (1 wt% of aq. phase) and castor oil to water volume ratios of 30/70, 50/50, 70/30 and 90/10 (left to right). **a** Picture taken at time 0 h; **b** picture taken after 24 h; **c** corresponding microscopic pictures of the emulsions at time 0 h; **d** microscopic pictures taken after 24 h; Scale bars represent 500 µm

Demulsification of the emulsions by an external magnet and recovery of the magnetic CNCs

It was demonstrated in this study that Pickering emulsions stabilized by the CNC/Fe_3O_4 NPs have controlled stability and are breakable by an external magnetic field on demand (Lin et al. 2016), although the conditions have to be carefully adjusted to ensure adequate control. Figure 9 depicts the effect of an external magnetic field on emulsions prepared with WCNC/Fe_3O_4 of 1:4 (1 wt% of aq. phase) with castor oil to water volume ratios of 30/70, 50/50, 70/30, and 90/10. For O/W emulsions containing castor oil percentages of 30% and 50% (Fig. 9a), the oil droplets were pulled by the magnet, but redispersed when the magnet was removed (Fig. 9b), indicating the emulsions were very stable. The micrographs were taken after removing the magnet, and confirmed oil droplets remained dispersed in water. Although at the 50/50 ratio, the oil droplets appeared larger than before being exposed to the magnet. Generally, particles make Pickering emulsions more stable to coalescence compared to surfactant stabilized systems, because the energy required for desorption

of the particles from the interface is very high (10^2-10^4 k_BT). The stability of the emulsions depends on the wettability of the particles that can irreversibly adsorb onto the interface (Akartuna et al. 2008; Ye et al. 2018), but also on the oil to water ratio (Parajuli et al. 2019). Further investigations are required to destabilize O/W emulsions with 50% or less completely oil content, including the wettability of the NPs, calculation of desorption energy, and intensity of the magnetic field.

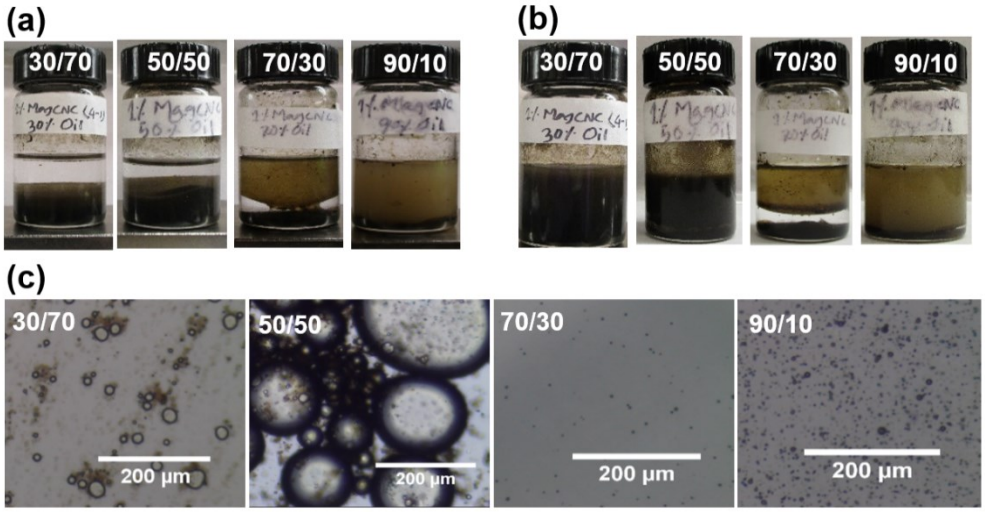

Fig. 9 Effect of an external magnetic field on castor oil and water Pickering emulsions prepared with castor oil to water volume ratios of 30/70, 50/50, 70/30, and 90/10 and stabilized by WCNC/Fe_3O_4 of 1:4 NPs (1 wt% of aqueous phase). **a** Picture of all the emulsions sitting on a magnet; **b** pictures of the vials after removing the magnet; **c** corresponding microscopy images of the emulsions after removing the magnet (samples were taken from the emulsion, or if no emulsion is present, the oil-rich phase)

The W/O emulsions with castor oil percentages of 70% and 90% (Fig. 9a), were readily broken by the magnet, and the NPs recovered. Although some droplets were still observed in the top oil phase (Fig. 9c), the results indicate successful destabilization of the emulsions by an external magnetic field. It is herein proposed that the force of the applied magnetic field, in addition to the effect of gravity, helps demulsify the O/W emulsions by bringing the droplets closer to each other, leading to coalescence. Emulsions prepared with BCNC/Fe_3O_4 NPs showed similar results during magnetic separation. The O/W emulsions did not break in the presence of a magnetic field, whereas W/O emulsions easily broke and the NPs were separated with the magnet (Fig. S13).

Recyclability of the magnetic cellulose nanocrystals

Recyclability of the recovered superparamagnetic NPs in castor oil/water emulsions was performed by periodic emulsification and demulsification. Figure 10 shows three cycles of emulsification and demulsification of the dispersions at 70% v/v castor oil, where the emulsion was stabilized by WCNC/Magnetite of 1:4 NPs and destabilized by magnet. The broken emulsions were re-stabilized by redispersing the NPs in the same oil water mixture by using a high shear mixture. At each cycle, the emulsion type was observed to be water in oil (w/o) and the time required for the

complete demulsification of each cycle was 4 hours. These recycled NPs can be useful to improve the economics and sustainability of processes or products involving Pickering emulsions. Some applications, where only temporary stability of the emulsions is required, may include low-energy separations, enhanced oil recovery, and drug delivery. The synthesized magnetite coated cellulose nanocrystals (CNC/Fe_3O_4) can be used to stabilize emulsions for a controlled period of time, demulsify on demand, and be recovered from the system with a magnetic field to be reused.

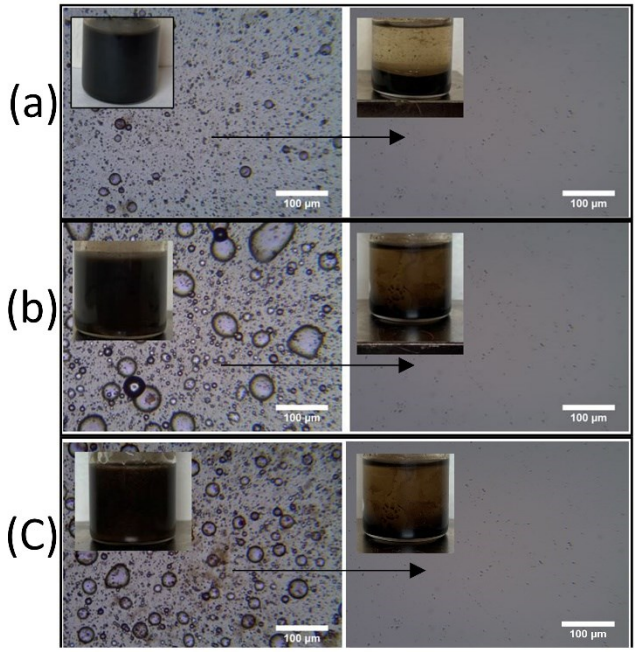

Fig. 10 Three cycles of emulsification and demulsification of castor oil/water emulsions at 70/30 oil to water ratio and stabilized by WCNC/Magnetite of 1:4 (1 wt% of aq. phase); **a** first cycle; **b** second cycle; and **c** third cycle; the microscopic pictures at the left were taken after stabilizing the emulsion and the pictures at the right were taken after magnetic separation.

The composite CNC/Fe_3O_4 NPs add the ability to stabilize both W/O and O/W emulsions; which are more resistant to creaming than emulsions without NPs and with CNCs only. The composite CNC/Fe_3O_4 NPs appear to have a higher affinity towards the interface compared to CNCs only. The CNC/Fe_3O_4 NPs are also responsive to an external magnetic field and thus can be broken at will with a magnet, which is not possible with the other emulsions.

Conclusion

Magnetite (Fe_3O_4) nanoparticle (NP) coated cellulose nanocrystals (CNC/Fe_3O_4) were successfully synthesized by a coprecipitation method with shorter wood pulp CNCs (WCNCs) and longer bacterial CNCs (BCNCs). The properties of the superparamagnetic CNC/Fe_3O_4 NPs were carefully optimized by changing the CNC to magnetite mass ratio (1:1, 1:2 and 1:4) during synthesis and used

to stabilize Pickering emulsions that can be broken at will upon application of an external magnetic field. It was found from TEM images and TGA that WCNC/Fe_3O_4 (1:4) and BCNC/Fe_3O_4 (1:4) had the highest Fe_3O_4 contents, 74.1 ± 6.1%, and 66.9 ± 5.1%, respectively. FT-IR and Raman spectroscopy suggested the interaction between Fe_3O_4 NPs and CNCs may be driven by hydrogen bonding interactions between the hydroxyl groups on the surfaces of both NPs. VSM studies depicted that the modified CNCs were superparamagnetic, showing no hysteresis, and having high saturation magnetizations of 60 emu/g for BCNC/Fe_3O_4 (1:4) and 56 emu/g for WCNC/Fe_3O_4 (1:4). Results suggest a larger saturation magnetization for the higher aspect ratio nanoparticles, although additional experimentation is still required on this regard. The colloidal stability in water at pH 7, of the hybrid NPs, decreased as the magnetite load was increased. Visual inspection and UV-vis spectroscopy at pH 7 indicated that bare Fe_3O_4 precipitated within one day of preparation, while the 1:2 and 1:4 NPs took approximately a week to precipitate at 0.005 wt%. The 1:1 hybrid NPs were stable for 1 week at the same concentration.

Properties of both NPs were successfully combined in the hybrid material, where the Fe_3O_4 lowered the colloidal stability of the CNCs and provided superparamagnetic properties. In the meantime, the flocculated CNCs provided an efficient means for emulsification of the oil/water mixtures. At a mass ratio of 1:4 the CNC/Fe_3O_4 NPs had limited colloidal stability and large saturation magnetization, allowing first the stabilization of Pickering emulsions and then the disruption of the Pickering effect by an external magnetic field. Aqueous dispersions containing 1 wt% of either WCNC/Fe_3O_4 (1:4) or BCNC/Fe_3O_4 (1:4) were readily emulsified with castor oil and remained stable for over 24 h. For both types of hybrid NPs, at oil concentrations of 30% and 50%, the emulsions were oil-in-water (O/W) and were too stable to be broken by an external magnet. On the contrary, at oil concentrations of 70% and 90%, the emulsions were identified as water-in-oil (W/O) and were readily broken by an external magnet. In these cases, the CNC/Fe_3O_4 NPs were also recovered and recycled. The synthesized hybrid NPs can potentially be used in applications including low-energy separations, drug delivery, and enhanced oil recovery to stabilize emulsions for controlled amounts of time and destabilize them at will.

Acknowledgments This work was funded in part by the National Science Foundation under grants 1704897 and 1705331. We thank Drs. Ahmed Al-Ostaz and Xiaobing Li for TGA and FTIR use, and Dr. Gabriela Romero Uribe for the Zetasizer use.

References

Abitbol T, Kloser E, Gray DG (2013) Estimation of the surface sulfur content of cellulose nanocrystals prepared by sulfuric acid hydrolysis. Cellulose 20:785–794. https://doi.org/10.1007/s10570-013-9871-0

Akartuna I, Studart AR, Tervoort E, et al (2008) Stabilization of Oil-in-Water Emulsions by Colloidal Particles Modified with Short Amphiphiles. Langmuir 24:7161–7168. https://doi.org/10.1021/la800478g

AlYousef ZA, Almobarky MA, Schechter DS (2018) The effect of nanoparticle aggregation on surfactant foam stability. J Colloid Interf Sci 511:365–373. https://doi.org/10.1016/j.jcis.2017.09.051

Barnes G, Gentle I (2011) Interfacial Science: An Introduction. OUP Oxford

Benaissi K, Johnson L, Walsh DA, Thielemans W (2010) Synthesis of platinum nanoparticles using cellulosic reducing agents. Green Chem 12:220–222. https://doi.org/10.1039/B913218J

Bendahou A, Hajlane A, Dufresne A, et al (2015) Esterification and amidation for grafting long aliphatic chains on to cellulose nanocrystals: a comparative study. Res Chem Intermediat 41:4293–4310. https://doi.org/10.1007/s11164-014-1530-z

Berg JC (2010) An Introduction to Interfaces and Colloids: The Bridge to Nanoscience. World Scientific

Cao S-L, Li X-H, Lou W-Y, Zong M-H (2014) Preparation of a novel magnetic cellulose nanocrystal and its efficient use for enzyme immobilization. J Mater Chem B 2:5522–5530. https://doi.org/10.1039/C4TB00584H

Chen L, Berry RM, Tam KC (2014) Synthesis of β-Cyclodextrin-Modified Cellulose Nanocrystals (CNCs)@Fe3O4@SiO2 Superparamagnetic Nanorods. ACS Sustain Chem Eng 2:951–958. https://doi.org/10.1021/sc400540f

Cîrcu M, Nan A, Borodi G, et al (2016) Refinement of Magnetite Nanoparticles by Coating with Organic Stabilizers. Nanomaterials-Basel 6:228. https://doi.org/10.3390/nano6120228

Dhar P, Kumar A, Katiyar V (2016) Magnetic Cellulose Nanocrystal Based Anisotropic Polylactic Acid Nanocomposite Films: Influence on Electrical, Magnetic, Thermal, and Mechanical Properties. ACS Appl Mater Inter 8:18393–18409. https://doi.org/10.1021/acsami.6b02828

Dhar P, Kumar A, Katiyar V (2015) Fabrication of cellulose nanocrystal supported stable Fe(0) nanoparticles: a sustainable catalyst for dye reduction, organic conversion and chemo-magnetic propulsion. Cellulose 22:3755–3771. https://doi.org/10.1007/s10570-015-0759-z

Dong S, Bortner MJ, Roman M (2016) Analysis of the sulfuric acid hydrolysis of wood pulp for cellulose nanocrystal production: A central composite design study. Ind Crop Prod 93:76–87. https://doi.org/10.1016/j.indcrop.2016.01.048

Dong XM, Revol J-F, Gray DG (1998) Effect of microcrystallite preparation conditions on the formation of colloid crystals of cellulose. Cellulose 5:19–32

Eskandar NG, Simovic S, A. Prestidge C (2007) Synergistic effect of silica nanoparticles and charged surfactants in the formation and stability of submicron oil-in-water emulsions. Phys Chem Chem Phys 9:6426–6434. https://doi.org/10.1039/B710256A

Gray DG (2008) Transcrystallization of polypropylene at cellulose nanocrystal surfaces. Cellulose 15:297–301. https://doi.org/10.1007/s10570-007-9176-2

Kalashnikova I, Bizot H, Cathala B, Capron I (2012) Modulation of Cellulose Nanocrystals Amphiphilic Properties to Stabilize Oil/Water Interface. Biomacromolecules 13:267–275. https://doi.org/10.1021/bm201599j

660 Kalashnikova I, Bizot H, Cathala B, Capron I (2011) New Pickering Emulsions Stabilized
661 by Bacterial Cellulose Nanocrystals. Langmuir 27:7471–7479.
662 https://doi.org/10.1021/la200971f

663 Keera ST, El Sabagh SM, Taman AR (2018) Castor oil biodiesel production and
664 optimization. Egypt J Pet 27:979–984. https://doi.org/10.1016/j.ejpe.2018.02.007

665 Kumar SV, Bafana AP, Pawar P, et al (2018) High conversion synthesis of <10 nm
666 starch-stabilized silver nanoparticles using microwave technology. Sci Rep-UK
667 8:1–10. https://doi.org/10.1038/s41598-018-23480-6

668 Lin Z, Zhang Z, Li Y, Deng Y (2016) Recyclable magnetic-Pickering emulsion liquid
669 membrane for extracting phenol compounds from wastewater. J Mater Sci
670 51:6370–6378. https://doi.org/10.1007/s10853-016-9933-4

671 Lopez JA, González F, Bonilla FA, et al (2010) Synthesis and characterization of Fe3O4
672 magnetic nanofluid. Rev Latinoam de Metal y Mater 30:60–66

673 Low LE, Tan LT-H, Goh B-H, et al (2019) Magnetic cellulose nanocrystal stabilized
674 Pickering emulsions for enhanced bioactive release and human colon cancer
675 therapy. Int J Biol Macromol 127:76–84.
676 https://doi.org/10.1016/j.ijbiomac.2019.01.037

677 Low LE, Tey BT, Ong BH, et al (2017) Palm olein-in-water Pickering emulsion
678 stabilized by Fe3O4-cellulose nanocrystal nanocomposites and their responses to
679 pH. Carbohyd Polym 155:391–399. https://doi.org/10.1016/j.carbpol.2016.08.091

680 Mahmoud KA, Lam E, Hrapovic S, Luong JHT (2013) Preparation of Well-Dispersed
681 Gold/Magnetite Nanoparticles Embedded on Cellulose Nanocrystals for Efficient
682 Immobilization of Papain Enzyme. ACS Appl Mater Inter 5:4978–4985.
683 https://doi.org/10.1021/am4007534

684 Midmore BR (1998) Preparation of a novel silica-stabilized oil/water emulsion. Colloid
685 Surface A 132:257–265. https://doi.org/10.1016/S0927-7757(97)00094-0

686 Nypelö T, Rodriguez-Abreu C, Kolen'ko YV, et al (2014a) Microbeads and Hollow
687 Microcapsules Obtained by Self-Assembly of Pickering Magneto-Responsive
688 Cellulose Nanocrystals. ACS Appl Mater Inter 6:16851–16858.
689 https://doi.org/10.1021/am504260u

690 Nypelö T, Rodriguez-Abreu C, Rivas J, et al (2014b) Magneto-responsive hybrid
691 materials based on cellulose nanocrystals. Cellulose 21:2557–2566.
692 https://doi.org/10.1007/s10570-014-0307-2

693 Olsson RT, Samir MASA, Salazar-Alvarez G, et al (2010) Making flexible magnetic
694 aerogels and stiff magnetic nanopaper using cellulose nanofibrils as templates.
695 Nat Nanotechnol 5:584–588. https://doi.org/10.1038/nnano.2010.155

696 Parajuli S, Alazzam O, Wang M, et al (2020) Surface properties of cellulose nanocrystal
697 stabilized crude oil emulsions and their effect on petroleum biodegradation.
698 Colloid Surface A 596:124705. https://doi.org/10.1016/j.colsurfa.2020.124705

699 Parajuli S, Dorris AL, Middleton C, et al (2019) Surface and Interfacial Interactions in
700 Dodecane/Brine Pickering Emulsions Stabilized by the Combination of Cellulose
701 Nanocrystals and Emulsifiers. Langmuir 35:12061–12070.
702 https://doi.org/10.1021/acs.langmuir.9b01218

Roman M (2015) Toxicity of Cellulose Nanocrystals: A Review. Ind Biotechnol 11:25–33. https://doi.org/10.1089/ind.2014.0024

Saien J, Bamdadi H, Daliri S (2015) Liquid–liquid extraction intensification with magnetite nanofluid single drops under oscillating magnetic field. J Ind Eng Chem 21:1152–1159. https://doi.org/10.1016/j.jiec.2014.05.028

Salas C, Nypelö T, Rodriguez-Abreu C, et al (2014) Nanocellulose properties and applications in colloids and interfaces. Curr Opin Colloid In 19:383–396. https://doi.org/10.1016/j.cocis.2014.10.003

Sanchez-Garcia MD, Lagaron JM (2010) On the use of plant cellulose nanowhiskers to enhance the barrier properties of polylactic acid. Cellulose 17:987–1004. https://doi.org/10.1007/s10570-010-9430-x

Shebanova ON, Lazor P (2003) Raman spectroscopic study of magnetite (FeFe2O4): a new assignment for the vibrational spectrum. J Solid State Chem 174:424–430. https://doi.org/10.1016/S0022-4596(03)00294-9

Soares SF, Fernandes T, Trindade T, Daniel-da-Silva AL (2019) Trimethyl Chitosan/Siloxane-Hybrid Coated Fe3O4 Nanoparticles for the Uptake of Sulfamethoxazole from Water. Molecules 24:1958. https://doi.org/10.3390/molecules24101958

Tian C, Fu S, Lucia LA (2015) Magnetic Cu0.5Co0.5Fe2O4 ferrite nanoparticles immobilized in situ on the surfaces of cellulose nanocrystals. Cellulose 22:2571–2587. https://doi.org/10.1007/s10570-015-0658-3

Ureña-Benavides EE, Ao G, Davis VA, Kitchens CL (2011) Rheology and Phase Behavior of Lyotropic Cellulose Nanocrystal Suspensions. Macromolecules 44:8990–8998. https://doi.org/10.1021/ma201649f

Ureña-Benavides EE, Brown PJ, Kitchens CL (2010) Effect of Jet Stretch and Particle Load on Cellulose Nanocrystal−Alginate Nanocomposite Fibers. Langmuir 26:14263–14270. https://doi.org/10.1021/la102216v

Ureña-Benavides EE, Lin EL, Foster EL, et al (2016) Low Adsorption of Magnetite Nanoparticles with Uniform Polyelectrolyte Coatings in Concentrated Brine on Model Silica and Sandstone. Ind Eng Chem Res 55:1522–1532. https://doi.org/10.1021/acs.iecr.5b03279

Wang H, Lin K-Y, Jing B, et al (2013) Removal of oil droplets from contaminated water using magnetic carbon nanotubes. Water Res 47:4198–4205. https://doi.org/10.1016/j.watres.2013.02.056

Wardhono EY, Wahyudi H, Agustina S, et al (2018) Ultrasonic Irradiation Coupled with Microwave Treatment for Eco-friendly Process of Isolating Bacterial Cellulose Nanocrystals. Nanomaterials-Basel 8:859. https://doi.org/10.3390/nano8100859

Xue Z, Foster E, Wang Y, et al (2014) Effect of Grafted Copolymer Composition on Iron Oxide Nanoparticle Stability and Transport in Porous Media at High Salinity. Energ Fuel 28:3655–3665. https://doi.org/10.1021/ef500340h

Ye H-M, Wang C-S, Zhang Z-Z, Yao S-F (2018) Effect of cellulose nanocrystals on the crystallization behavior and enzymatic degradation of poly(butylene adipate). Carbohyd Polym 189:99–106. https://doi.org/10.1016/j.carbpol.2018.02.025

746 Zhou J, Qiao X, Binks BP, et al (2011) Magnetic Pickering Emulsions Stabilized by
747 Fe3O4 Nanoparticles. Langmuir 27:3308–3316.
748 https://doi.org/10.1021/la1036844

749